Coupling of morphological instability and kinetic instability: Chemical waves in hydrogen oxidation on a bimetallic Ni/Rh(111) surface

Mathias Homann,[1] Bernhard von Boehn,[1] Mauricio Prieto,[2,3] Daniel M. Gottlob,[2] Liviu C. Tănase,[2,3] Thomas Schmidt,[2,3] Francesca Genuzio,[4] Tevfik O. Menteş,[4] Andrea Locatelli,[4] and Ronald Imbihl[1,*]

[1]*Institut für Physikalische Chemie und Elektrochemie, Leibniz-Universität Hannover, Callinstrasse 3A, D-30167 Hannover, Germany*

[2]*Department of Chemical Physics, Fritz-Haber-Institut der Max-Planck Gesellschaft, Faradayweg 4–6, D-14195 Berlin, Germany*

[3]*Department of Interface Science, Fritz-Haber-Institut der Max-Planck Gesellschaft, Faradayweg 4–6, D-14195 Berlin, Germany*

[4]*Elettra - Sincrotrone Trieste, S.C.p.A., S.S. 14, km 163.5 in AREA Science Park, 34149 Basovizza, Trieste, Italy*

(Received 21 January 2020; revised 30 December 2020; accepted 17 March 2021; published 2 April 2021)

The oxidation and reduction of a bimetallic Ni/Rh model catalyst during the water forming $O_2 + H_2$ reaction is studied with low-energy electron microscopy, microspot-low-energy electron diffraction, and x-ray photoemission electron microscopy. Oxidation of a submonolayer Ni film results in the formation of three-dimensional (3D) NiO nanoparticles. Reduction of 3D-NiO in H_2 produces a dispersed two-dimensional film of metallic Ni. Chemical waves during the $O_2 + H_2$ reaction involve a cyclic transformation between 3D-NiO and 2D-NiO.

DOI: 10.1103/PhysRevMaterials.5.045002

Bimetallic catalysts play a prominent role in heterogeneous catalysis [1]. Whereas quantum chemical methods can reliably predict the adsorption behavior of bimetallic surfaces, little is known about the dynamics of these systems under reaction conditions [2–4]. Oxidation and reduction of a metal are fundamental chemical processes that can occur in such systems. Such simple chemical processes can lead to complex dynamical behavior as best illustrated by the occurrence of chemical waves in the $O_2 + H_2$ reaction on a bimetallic Rh(111)/Ni surface [5–8]. The chemical waves in this system were shown to be connected to a periodic oxidation and reduction of the Ni [5]. Such an oxidation/reduction process well known under the "oxide model" is a standard mechanism to explain the occurrence of kinetic oscillations in catalytic oxidation reactions on Pt, Pd, Ir, and Ni at elevated pressure [9–13]. Here we show that at the core of the kinetic instability leading to chemical waves on Ni/Rh(111) is a morphological instability as oxidation and reduction are connected with a reversible wetting of the substrate.

We investigate a bimetallic model catalyst consisting of ultrathin Ni layers supported on a Rh(111) surface. Under oxidizing conditions Ni can form a three-dimensional bulk oxide (3D-NiO) [14]. Yet, at submonolayer Ni coverage, two-dimensional Ni oxides (2D-NiO) can also develop, with both 2D and 3D oxides having the same 1:1 Ni/O composition [15–17]. The main obstacle in resolving chemical processes on a nanoscale is that the most established spectroscopic methods provide chemical and structural information on a global scale, but neglect any spatial structure. To overcome these limitations, we employ here x-ray photoemission electron microscopy (XPEEM) and spectroscopic low-energy electron microscopy (SPELEEM), a technique that combines the high spatial resolution of an electron microscope with the possibility to extract local chemical and structural information from a small area of about 1 μm diameter.

The experiments have been conducted at the SMART beamline at the synchrotron light source BESSY II of the Helmholtz Centre Berlin for Materials and Energy [18], and at the Nanospectroscopy beamline at Elettra, using the ELMITEC SPELEEM III microscope [19]. Both microscopes are energy filtered LEEM/PEEM instruments combining microscopy, diffraction, and spectroscopy techniques for comprehensive characterization [18,20]. To decipher the excitation mechanism behind the chemical waves on Ni/Rh(111) during the $O_2 + H_2$ reaction, we characterize in a first step the oxidation of a metallic Ni film in oxygen, and the reduction of 3D NiO particles. In a second step, we expose the Ni/Rh(111) model catalyst to reaction conditions and monitor the Ni oxidation / reduction dynamics *in situ*.

For a calibration of the Ni coverage the Ni $3p$ signal is recorded as a function of deposition time (Supplemental Material, Fig. S1), using the change in the slope as mark for completion of one monolayer (ML) [21]. Exposure of 0.8 ML of Ni supported on Rh(111) and subsequent heating in 5×10^{-8} mbar O_2 at $T = 780$ K for 25 min leads to coexisting 2D- and 3D-Ni oxide, as demonstrated by the LEEM image in Fig. 1 [21]. μLEED reveals three distinct phases: 3D-NiO(100) crystallites grown epitaxially on Rh(111) with the LEED spots stemming from the (100) facets, 2D-NiO identified by a (6×1) pattern and finally a (1×1) phase with very weak (2×2) spots representing the oxygen covered Rh(111) substrate. The weak intensity results from the measuring temperature of 780 K being above an order-disorder transition of the (2×2)-O adsorbate phase.

Ni $3p$, O $1s$, and Rh $3d_{5/2}$ XPEEM images of the oxidized surface are shown in Fig. 2. Analysis of the XPEEM spectra shows that the Rh(111) surface surrounding the 3D-NiO particles contains less than 10% of Ni. Apparently, the oxidation favors Rh dewetting and growth of Ni oxide islands. From the

*Corresponding author: imbihl@pci.uni-hannover.de

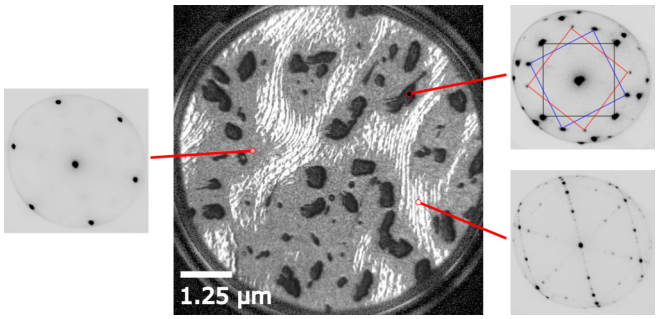

FIG. 1. Formation of three phases upon exposure of 0.8 ML Ni on Rh(111) to oxygen at $T = 780$ K as demonstrated by a LEEM image (middle). Selected areas of approximately 1 μm in diameter indicated by red lines are characterized by μLEED. The LEED patterns show a (1 × 1) (left), a (1 × 1) with additional spots belonging to the NiO(100) surface (top right, rotational domains are indicated), and a (6 × 1) of 2D-NiO (bottom right). Illumination apertures are used to minimize surface damage by the probing electron beam. Adsorption of O_2 : $p(O_2) = 5 \times 10^{-8}$ mbar. $t = 1500$ s; LEEM field of view (FOV): 7.5 μm, $E = 12$ eV; μLEED: $E = 51$ eV.

shadow length of the smallest 3D-NiO islands visible in the Ni 3p image, we estimate a height of 30–50 nm for the tallest

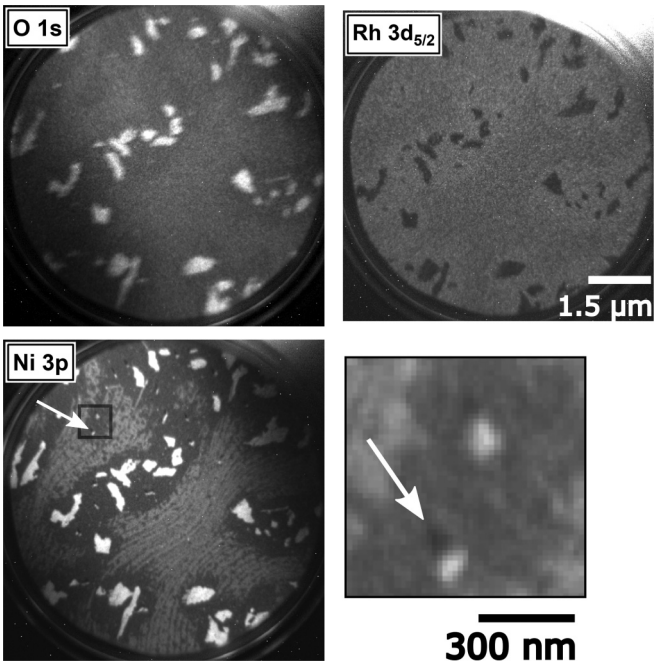

FIG. 2. Ni 3p, O 1s, and Rh 3$d_{5/2}$ XPEEM images from a Rh(111) surface promoted with 0.8 ML Ni, which was oxidized at 780 K. The images display a different surface region to that shown in Fig. 1. The bright objects in the O 1s (top left) and Ni 3p (bottom left) images are 3D-NiO particles. The particles are surrounded by a Ni-depleted region, appearing darker in the Ni 3p image. The 2D-NiO regions show up in an intermediate intensity level. An enlarged section of the Ni 3p image (bottom right) shows a shadowing of the photon beam by a tall 3D-NiO island. The ratio of the Ni 3p XPS intensity, normalized to the Rh 3d signal, from different regions on the surface is 3D-NiO: 2D-NiO: Ni-depleted area $= 44 \pm 9 : 6.6 \pm 2.2 : 1.3 \pm 0.6$. Photon energy: 150 eV (Ni 3p) and 650 eV (O 1s and Rh 3d).

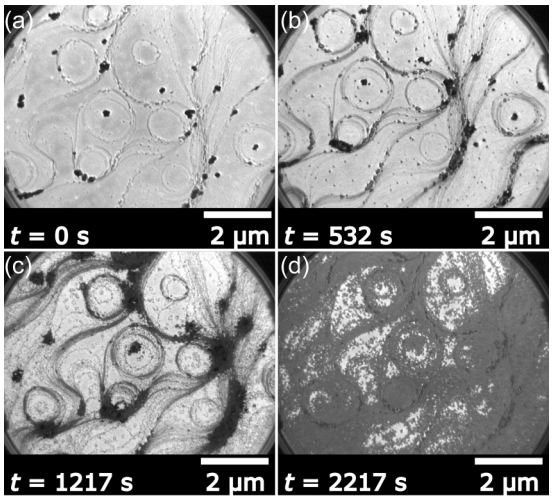

FIG. 3. Spreading of a 2D metallic Ni film during the reduction of 3D-NiO with hydrogen. Prior to hydrogen exposure, the 0.8 ML Ni film was oxidized at 800–830 K in 5×10^{-8} mbar oxygen. Shown are LEEM images recorded during heating the sample up in 5×10^{-8} mbar H_2 at (a) 540–570 K, (b) 590–620 K, and (c), (d) 640–670 K. LEEM $E = 12$ eV. (Video in the Supplemental Material S2).

3D-NiO particles. The average thickness of the other 3D-NiO islands, calculated from the attenuation of the Rh 3$d_{5/2}$ signal, is 0.8 nm, roughly corresponding to two lattice constants of NiO (for details, refer to the Supplemental Material) [21,22]. Please note that the region surrounding the 3D-NiO particles is not covered by 2D-NiO, but is depleted of Ni. This indicates that the growing 3D-NiO acts as a sink for 2D-NiO.

The relative amount of 3D-NiO and 2D-NiO depends sensitively on the temperature at which the Ni film is oxidized and on the oxygen pressure. At T < 700 K, initially mainly 2D-NiO is observed, whereas beyond 850 K preferentially 3D-NiO develops. When the oxidation is conducted at $T =$ 800–830 K and with $p(O_2) = 5 \times 10^{-8}$ mbar, we exclusively observed the formation of 3D-NiO particles with diameters of about 100–200 nm, which are surrounded by a (2 × 2)-O adlayer (Supplemental Material, Fig. S2) [21].

In the following, we study the reduction behavior of 3D-NiO on Rh(111) created by oxidizing the Ni/Rh(111) surface at 800–830 K. From the amount of Ni initially present and from the fraction of the surface covered by NiO islands we estimate an average height of 5.9 nm for the 3D-NiO particles initially present on the surface shown in Fig. 3, which had been oxidized at 800–830 K (please refer to the Supplemental Material) [21]. This value of 5.9 nm is larger than that obtained for the surface shown in Figs. 1 and 2, which had been oxidized at 780 K, where the majority of the islands did not exceed 1 nm in height. We attribute this difference to the lower temperature used in the experiment of Figs. 1 and 2, resulting in an incomplete transformation of the Ni film into 3D-NiO, i. e., much broader and less tall 3D-NiO islands.

To initiate reduction, the surface is heated up in H_2 starting at room temperature. The heating ramp (6 K/min) is stopped at $T \approx$ 640–670 K. The LEEM images in Fig. 3 show that the reduction of the 3D-NiO particles is accompanied by a lateral

redistribution of Ni, which spreads as a homogeneous 2D-film on the Rh surface surrounding the NiO particles (Supplemental Material, Fig. S3, Video 1) [21]. The Ni free area and Ni covered area are separated by a sharp interface.

Ni 3p and O 1s XPEEM spectroscopy, acquired in a similar reduction experiment, demonstrates that the Ni film is metallic and contains only traces of oxygen. The x-ray photoemission spectroscopy (XPS) data indicate that the oxygen coverage on the surface is less than 7% of the Ni coverage. Moreover, oxygen is expected to be bound to the uncovered Rh surface, rather than to the Ni covered surface area. We estimate that, at the end of the reduction treatment after 1 h, 82 ± 5% of the surface area is covered by the 2D Ni film. At this point, the contrast between the 3D particles and the surrounding Ni film has completely vanished. The fact that this value matches the initial Ni coverage (80 ± 5% of a ML) indicates that the 2D-Ni film is one monolayer thick. Furthermore, one can confidently exclude that a substantial amount of Ni has diffused into the subsurface region. Since Rh and Ni are completely miscible in the bulk, this latter result appears surprising, but evidently an energy barrier exists preventing the penetration of the Rh substrate by Ni adatoms. At elevated temperature, on an adsorbate free surface, Ni atoms in fact diffuse into the bulk above ≈ 600 K, but in the presence of small amounts of oxygen, temperatures above ≈ 900 K are required for surface Ni atoms to penetrate the Rh bulk [6,23].

Chemical waves on ultrathin Ni films on Rh(111) have been extensively studied with PEEM in a pressure range from 10^{-5} to 10^{-4} mbar [7,8]. As demonstrated by *in situ* XPS, chemical waves are accompanied by a cyclic formation and reduction of 3D-NiO [5,6]. However, scanning photoelectron microscopy could not detect 3D-NiO particles, likely due to insufficient lateral resolution (0.1 μm).

In the 10^{-6} mbar range, chemical waves can be followed *in situ* with LEEM. On a surface with 0.8 ML Ni, the waves can be initiated in the 10^{-6} mbar range at $T = 750$–770 K, at a ratio of $p(O_2)/p(H_2) = 1.1$. Since the few μm large field of view (FOV) in LEEM is small compared to the dimensions of a target pattern, which typically are around several hundred μm at 10^{-6} mbar, LEEM detects only the local variations on the surface as a chemical wave passes the area probed by LEEM. At an electron energy of 12 eV, the reduced surface appears brighter than the oxidized surface. The excursions in the integral LEEM intensity in Fig. 4(a) consequently reflect reduction pulses, i. e., a temporary change from the oxidized state into a reduced state of the surface.

The oxidized surface displays a complex morphology. In Fig. 4(b) the 3D-NiO islands can be recognized as small bright dots. A reduction pulse transforms this surface into a regular domain structure, clearly exhibiting a threefold symmetry as demonstrated by Fig. 4(c). The appearance of this structure is shown to be due to the formation of three rotationally equivalent (6 × 1) domains of 2D-NiO (Supplemental Material, Fig. S4, Video 2) [21]. This assignment is based on dark-field LEEM and LEED measurements performed *in situ* as well as in an additional adsorption experiment, where an identical domain structure was observed and characterized by LEED.

A closer inspection of Fig. 4(c) shows that the bright 3D-NiO islands observed on the oxidized surface also persist during a reduction pulse. Intensity profiles through the LEEM image displayed in Fig. 4(d), however, reveal that some of the bright spots during a reduction pulse lose intensity or become smaller. Evidently, only part of the 3D-NiO islands is

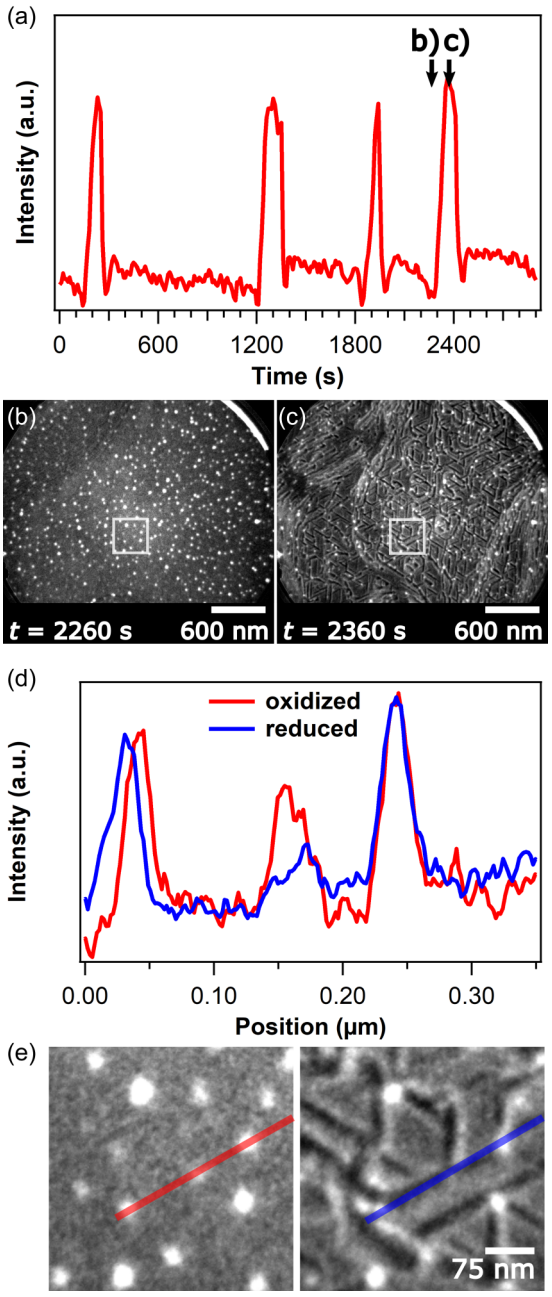

FIG. 4. Reversible transformation of 3D-NiO into 2D-NiO during chemical waves. (a) Variation of the LEEM intensity averaged over the FOV during propagation of chemical waves. The arrows mark the times where the snapshots in (b) and (c) were taken. LEEM images of the oxidized (b) and reduced state (c). (d) LEEM intensity profiles showing intensity changes for some of the 3D-NiO particles during chemical waves. (e) Enlarged sections of the LEEM images in (b) and (c) with the profiles used for (d) indicated. Note that the 3D-NiO imaged here as bright particles appears in Figs. 1 and 3 as dark islands due to different focusing adjustments. Experimental conditions: $p(O_2) = 1 \times 10^{-6}$ mbar; $p(H_2) = 9 \times 10^{-7}$ mbar, $T \approx$ 740– 770 K; LEEM E = 12 eV.

converted into 2D-NiO. Since 3D-NiO and 2D-NiO particles are known to both exhibit the same 1:1 Ni/O composition [15], a conversion alone does not involve an oxidation/reduction process. However, a previous *in situ* XPS study showed that metallic Ni is present during wave propagation, with the amount varying periodically with the pulses [5]. The transition from 3D-NiO to 2D-NiO is apparently enabled by the 2D-spreading of metallic Ni, as suggested by the reduction experiment of Fig. 3. In separate LEED experiments we verified that (i) the reduction of 3D-NiO leads to metallic Ni but not to 2D-NiO, and (ii) that 2D-NiO is formed when the metallic Ni film is reexposed to O_2. One can therefore construct the following excitation cycle for a reduction pulse: 3D-NiO → 2D-Ni metal → 2D-NiO → 3D-NiO. This cycle contains an oxidation and a reduction process.

Essential for the excitation mechanism to operate is that oxidation and reduction are not simply reverse processes in the sense that oxygen atoms, which had been removed by reduction, are simply replaced by oxygen adsorbing from the gas phase. A morphological change is involved in which the metallic Ni that is formed wets the metallic substrate. In LEEM the metallic Ni film is not visible during chemical waves but an indirect proof for the 2D spreading of Ni is the observation of the 2D-NiO phase. The 2D-NiO phase only forms when a Ni film is exposed to O_2 but not as a product of the reduction of 3D-NiO. Since metallic Ni is very reactive towards O_2, the spreading of a 2D-Ni film should considerably enhance the catalytic activity of the Ni/Rh(111) surface. One can therefore conclude that the dynamic instability that gives rise to chemical waves is due to the coupling of an oxidation/reduction process with a reversible wetting of the substrate [24].

In earlier papers it has been suspected that the reversible formation of subsurface Ni plays a key role in the excitation mechanism [5,8]. Since Ni on Rh(111) increases the surface energy, metallic Ni is expected to have a tendency to penetrate into the Rh bulk [25]. Due to the higher affinity of Ni to oxygen, an oxygen covered surface should attract Ni dissolved in the Rh bulk to segregate back to the surface. The reversible formation of subsurface Ni should cause a periodic change in the catalytic activity of the surface [5,8]. In fact, at elevated temperature, above ≈ 900 K, the initially deposited Ni on Rh(111) starts to diffuse into the Rh bulk [6]. Under the milder conditions at which chemical waves occur, however, no substantial loss of surface Ni occurs during reduction of NiO as clearly demonstrated by the reduction experiment displayed in Fig. 3. It is therefore unlikely that the reversible formation of subsurface Ni plays a decisive role in the excitation mechanism of chemical waves. Surprisingly, alloying accordingly plays practically no role in oxidation and reduction on the bimetallic surface but the processes are controlled by interfacial energies.

In summary, we have shown that reduction of nanosized 3D-NiO particles proceeds via spreading of a 2D metallic Ni film but reoxidation of the 2D-Ni film to 3D-NiO particles involves the formation of 2D-NiO as intermediate. During chemical waves in this system a periodic transformation of 3D-NiO into 2D-NiO and vice versa occurs so that an excitation cycle 3D-NiO → 2D-Ni metal → 2D-NiO → 3D-NiO can be constructed. The morphological instability that is associated with oxidation and reduction is considered to be an essential part of the excitation/oscillation mechanism in this system and probably of other systems whose nonlinear properties are described by the "oxide model".

B. von Boehn thanks the Department of Inorganic Chemistry of the Fritz Haber Institute of the Max Planck Society for financial support. The authors also thank the Helmholtz-Center Berlin for Materials and Energy (HZB) for the allocation of synchrotron radiation beamtime.

The manuscript was written through contributions of all authors. All authors have given approval to the final version of the manuscript.

The authors declare no competing financial interest.

[1] J. H. Sinfelt, Springer Ser. Surf. Sci. **5**, 19 (1986).
[2] A. Gross, Top. Catal. **37**, 29 (2006).
[3] J. K. Nørskov, F. Abild-Pedersen, F. Studt, and T. Bligaard, PNAS **108**, 937 (2011).
[4] F. Tao, M. E. Grass, Y. Zhang, D. R. Butcher, J. R. Renzas, Z. Liu, J. Y. Chung, B. S. Mun, M. Salmeron, and G. A. Somorjai, Science **322**, 932 (2008).
[5] T. Smolinsky, M. Homann, B. von Boehn, L. Gregoratti, M. Amati, M. Al Hada, H. Sezen, and R. Imbihl, J. Chem. Phys. **148**, 154705 (2018).
[6] T. Smolinsky, B. Von Boehn, and R. Imbihl, J. Chem. Phys. **148**, 154704 (2018).
[7] T. Smolinsky, M. Homann, and R. Imbihl, Phys. Chem. Chem. Phys. **18**, 970 (2016).
[8] F. Lovis, T. Smolinsky, A. Locatelli, M. A. Niño, and R. Imbihl, J. Phys. Chem. C **116**, 4083 (2012).
[9] B. C. Sales, J. E. Turner, and M. B. Maple, Surf. Sci. **114**, 381 (1982).
[10] V. V. Kaichev, A. Y. Gladky, I. P. Prosvirin, A. A. Saraev, M. Hävecker, A. Knop-Gericke, R. Schlögl, and V. I. Bukhtiyarov, Surf. Sci. **609**, 113 (2013).
[11] S. L. Lane and D. Luss, Phys. Rev. Lett. **70**, 830 (1993).
[12] V. Y. Bychkov, Y. P. Tulenin, M. M. Slinko, Y. A. Gordienko, and V. N. Korchak, Catal. Lett. **148**, 653 (2018).
[13] A. M. Gänzler, M. Casapu, A. Boubnov, O. Müller, S. Conrad, H. Lichtenberg, R. Frahm, and J.-D. Grunwaldt, J. Catal. **328**, 216 (2015).
[14] H. Zhang, W. Wang, M. Chen, and H. Wan, Appl. Surf. Sci. **439**, 569 (2018).
[15] T. Franz, J. Zabloudil, F. Mittendorfer, L. Gragnaniello, G. Parteder, F. Allegretti, S. Surnev, and F. P. Netzer, J. Phys. Chem. Lett. **3**, 186 (2012).
[16] L. Gragnaniello, F. Allegretti, R. R. Zhan, E. Vesselli, E. Braldi, G. Comelli, S. Surnev, and F. P. Netzer, Surf. Sci. **611**, 86 (2013).

[17] G. Parteder, F. Allegretti, M. Wagner, M. G. Ramsey, S. Surnev, and F. P. Netzer, J. Phys. Chem. C **112**, 19272 (2008).

[18] T. Schmidt, H. Marchetto, P. L. Levesque, U. Groh, F. Maier, D. Preikszas, P. Hartel, R. Spehr, G. Lilienkamp, W. Engel *et al.*,, Ultramicroscopy **110**, 1358 (2010).

[19] T. O. Menteş, G. Zamborlini, A. Sala, and A. Locatelli, Beilstein J. Nanotechnol. **5**, 1873 (2014).

[20] T. Schmidt, A. Sala, H. Marchetto, E. Umbach, and H.-J. Freund, Ultramicroscopy **126**, 23 (2013).

[21] See Supplemental Material at http://link.aps.org/supplemental/10.1103/PhysRevMaterials.5.045002 for details on the Ni coverage calibration (Fig. S1), on the oxide thickness estimation from Rh $3d_{5/2}$ XPS signal damping and XPEEM shadow length, on the Ni mass balance in the reduction experiment, on XPEEM of formation and reduction of 3D-NiO (Figs. S2, S3), on *in situ* dark field imaging of the 2D-NiO/(6 × 1) phase during chemical waves (Fig. S4) and two videos with Video 1, showing the reduction of 3D -NiO particles in LEEM and Video 2, showing the development of a domain structure in LEEM during chemical waves.

[22] S. Tanuma, C. J. Powell, and D. R. Penn, Surf. Interf. Anal. **21**, 165 (1994).

[23] A. Wander, C. J. Barnes, L. D. Mapledoram, and D. A. King, Surf. Sci. **281**, 42 (1993).

[24] S. Surnev, J. Schoiswohl, G. Kresse, M. G. Ramsey, and F. P. Netzer, Phys. Rev. Lett. **89**, 246101 (2002).

[25] A. Christensen, A. V. Ruban, P. Stoltze, K. W. Jacobsen, H. L. Skriver, J. K. Norskov, and F. Besenbacher, Phys. Rev. B **56**, 5822 (1997).